Journal of Materials Chemistry

Cite this: *J. Mater. Chem.*, 2012, **22**, 9285

www.rsc.org/materials

PAPER

A new supramolecular POSS electroluminescent material†

Yu-Lin Chu, Chih-Chia Cheng,* Ya-Ping Chen, Ying-Chieh Yen and Feng-Chih Chang*

Received 5th January 2012, Accepted 7th March 2012
DOI: 10.1039/c2jm00095d

A new polyhedral oligomeric silsesquioxane (POSS) core star-like supramolecular blue-light electroluminescent material, 4-uracilbutyl-1-methylpyrene ether (U-PY)/octakis[dimethyl(*N*-(6-acetamidopyridin-2 yl))siloxy] silsesquioxane (ODAP-POSS) has been synthesized. This U-PY/ODAP-POSS contains eight pyrene chromophore arms formed through complementary uracil-diamidopyridine (U-DAP) pairs and exhibits high quantum efficiencies and good solution processing properties. The photoluminescence spectra of U-PY/ODAP-POSS (50/50) reveal that the color is stable after heating the sample at 150 °C for 1 h, in contrast, the pyrene/ODAP-POSS (50/50) shows significant thermal quenching. An electroluminescence (EL) device based on U-PY/ODAP-POSS exhibits higher maximum brightness and higher luminance efficiency relative to that of the U-PY. In addition, U-PY/ODAP-POSS also behaves as an effective dopant that enhances energy transfer from itself to MEH-PPV. The U-PY/ODAP-POSS-doped MEH-PPV blends exhibit high luminance efficiency, 1.45 times greater than MEH-PPV.

Introduction

In both DNA and RNA, hydrogen-bonding interactions have attracted a great deal of interest because of their novel structural organization.[1–3] The association of two complementary compounds with moderately strong and highly directional molecular recognition exhibits unique structures and properties, which cannot be obtained by the individual components. Numerous reports regarding the effect of the placement of supramolecular motifs on chain ends[4–7] and side chains[8–13] of polymers or small molecules on material properties have been reported. The poly(styrene-*co*-chloromethylstyrene) copolymer reported by Rotello[14–18] and the quadruple hydrogen-bonded ureidopyrimidone derivatives with donor–donor–acceptor–acceptor (DDAA) structure reported by Meijer, and co-workers[19–23] are representative cases of the side chain and chain ends types, respectively. Intensive research has been directed toward functional supramolecular systems to control the dimensionality and shape of self-assembled structures through molecular design, but it is still a challenge to control the supramolecule with secondary (and higher) bonding through specific interactions from different hydrogen-bonding motifs.

Recently, organic/inorganic hybrid nanocomposites based on polyhedral oligomeric silsesquioxanes (POSS) derivatives have attracted considerable interest[24–27] because they exhibit several advantageous properties resulting from the unique physical properties of POSS nanoparticles (NPs).[28–32] Through appropriate design of their architectures, POSS derivatives can be tailored for specific applications.[33–35] POSS macromolecules bearing the chromophore moieties provide the advantages of both small-molecule and polymer light-emitting materials (*i.e.*, high purity, solution processability and stability). The presence of POSS can improve quantum efficiencies, improve the thermal stability of the light-emitting materials, suppress the aggregation of chromophores, and enhance photoluminescence (PL) and electroluminescence (EL) performance.[36–45] Nevertheless, only a limited number of reports have appeared so far regarding POSS containing multiple hydrogen-bonding recognition sites[26,46] and no previous studies have been reported on the effect of hydrogen-bonded molecular recognition on the thermal, photophysical and electroluminescence properties based on the POSS containing non-covalently bonded chromophores.

In our previous study, we have reported the biocomplementary interactions of a DNA like side-chain homopolymer with alkylated nucleobases mediated by hydrogen-bonded thymine–adenine (T–A) base pairs.[47] Recently, we also reported that the polyhedral oligomeric silsesquioxane macromer, octakis[*N*-(6-aminopyridin-2-yl)-undecanamide-10-dimethyl-siloxy] silsesquioxane (POSS-C11-Py), containing eight diaminopyridine arms which is able to self-assemble into a physically crosslinked polymer-like structure through quadruple hydrogen bonding interactions between these arms.[46] In this study, we present the syntheses of 4-uracilbutyl-1-methylpyrene ether (U-PY) and octakis[dimethyl(*N*-(6-acetamidopyridin-2-yl))siloxy] silsesquioxane (ODAP-POSS), respectively. U-PY is able to interact with its complementary ODAP-POSS to form a star-like structure through complementary uracil–diamidopyridine (U–DAP)

Institute of Applied Chemistry, National Chiao Tung University, Hsinchu, Taiwan. E-mail: changfc@mail.nctu.edu.tw; chihchia.ac95g@nctu.edu.tw; Fax: +886-3-5131512; Tel: +886-3-5131512

† Electronic supplementary information (ESI) available. See DOI: 10.1039/c2jm00095d

pairing and exhibits improved solution processing, optical and electroluminescence (EL) properties. In addition, the U-PY/ODAP-POSS can act as an effective dopant to transfer energy to orange light-emitting poly(2-methoxy,5-(2′-ethyl-hexyloxy)-*p*-phenylene-vinylene) (MEH-PPV) and thus significantly enhances the device performance of MEH-PPV.

Results and discussion

Syntheses and molecular recognition studies of U-PY/ODAP-POSS complexes

We synthesized a new nanoparticle ODAP-POSS through a hydrosilation reaction (Scheme 1) between octakis(dimethylsiloxy)silsesquioxane and an alkene modified DAP compound, functionalized as a hydrogen bonding segment. ODAP-POSS was recovered in high yield (83%) and its molecular weight (M_w = 2995 g mol^{-1}, which matches almost exactly a single value of n = 8) was consistent with the structure of the molecule presented in the experimental section and in the Fig. S8.† ODAP-POSS is able to form complexes with U-PY through complementary U–DAP hydrogen bonding, which affords unique capabilities for forming well-ordered structures through bottom-up assembly of U-PY/ODAP-POSS complexes. In this article, we characterized the assembly behavior of these complexes using ^{1}H NMR and FTIR spectroscopy. The U-PY/ODAP-POSS was dissolved in d_2-tetrachloroethane at 25 °C to calculate the association constant (K_a) for the U–DAP complex (Fig. S1†). The chemical shift of the amide proton of uracil in the complex U-PY/ODAP-POSS was monitored to give a value of K_a of 36.8 M^{-1} from Benesi–Hildebrand plots (Fig. S2†). FT-IR spectra (Fig. 1) also reveal strong bands at 3273 cm^{-1} and 3211 cm^{-1} corresponding to hydrogen-bonded amide N–Hs in a 50/50 complex, indicating that interaction occurs through strong cooperative hydrogen bonding between U-PY and ODAP-POSS and results in highly special conformational changes in the solution and solid states.

Self-assembly of U-PY/ODAP-POSS in bulk state

Since U-PY and ODAP-POSS forms a star-like structure, the self-assemblies of these complexes were examined in the bulk state using differential scanning calorimetry (DSC) and wide-angle X-ray diffraction (WAXRD). TGA thermal degradation patterns of U-PY and PY are shown in Fig. 2. U-PY has a significantly higher $T_{d,5\%}$ (297 °C) as compared to PY (170 °C), indicating that the attachment of uracil moiety into the PY significantly enhances the thermal stability. Fig. S3 (a)† displays DSC traces for the U-PY/ODAP-POSS complexes where essential all composites give single glass transition temperature (T_g), indicating that the U-PY/ODAP-POSS are completely miscible. TGA thermal degradation patterns of U-PY/ODAP-POSS are shown in Fig. S3 (b);† Table S1† summarizes the thermal properties data, the $T_{d,5\%}$ for U-PY/ODAP-POSS complexes are slightly lower than U-PY. However, the $T_{d,40\%}$ values of U-PY/ODAP-POSS complexes showed a large increase in *thermal resistance*. In addition, the char yield of U-PY/ODAP-POSS complexes at 800 °C was close to the theoretical value, indicating its superior thermal stability. Fig. 3 shows WXRD diffraction patterns of U-PY/ODAP-POSS composites, displaying three

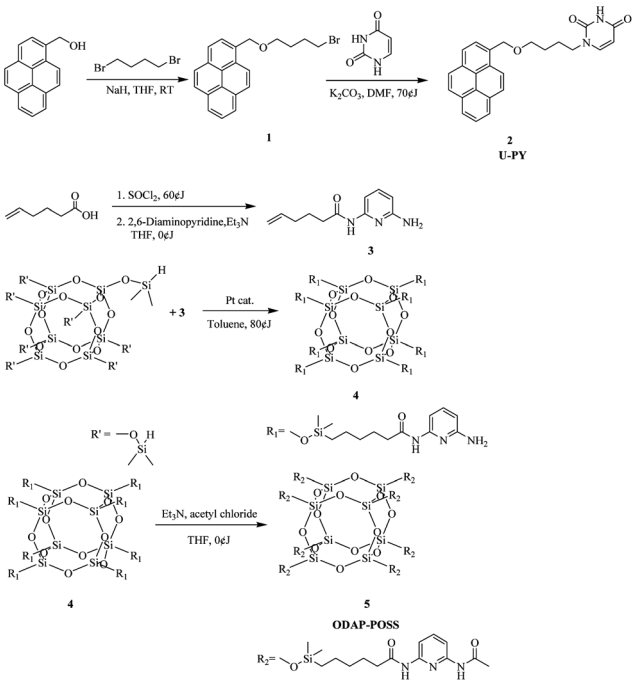

Scheme 1 Synthetic procedures used to obtain U-PY and ODAP-POSS.

reflection peaks at 9.0° (d = 0.98 nm), 26.9° (d = 0.33 nm) and 27.3° (d = 0.32 nm). The reflection peaks corresponding to d spacing of 0.33 nm and 0.32 nm are consistent with the presence of π–π stacking interactions in pyrene–pyrene and heterocyclic layers, respectively.[48–51] The d spacing of 0.98 nm suggests that there are stacks of the heterocyclics that are held together through U–U or DAP–U interactions within these interaction domains The pure ODAP-POSS exhibits a broad peak at 7.86° (1.12 nm) that is attributed to the formation of the complementary complex on the d-spacing of the ODAP-POSS.[46] Another peak at 18.1° (0.45 nm) corresponds to the inter- and intra-chain distances within the POSS moiety.[46] The DAP–DAP

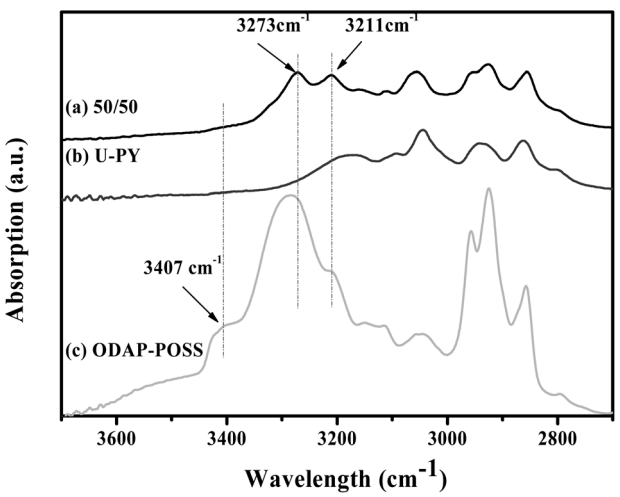

Fig. 1 FTIR spectra recorded at room temperature in the range of 2700–3700 cm^{-1} for U-PY/ODAP-POSS (50/50) (a), U-PY (b) and ODAP-POSS (c) in the solid state.

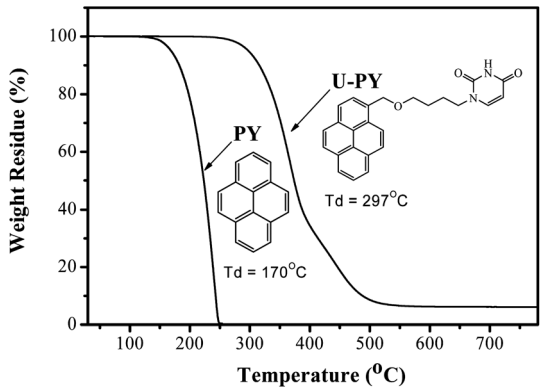

Fig. 2 TGA thermal degradation patterns for PY and U-PY.

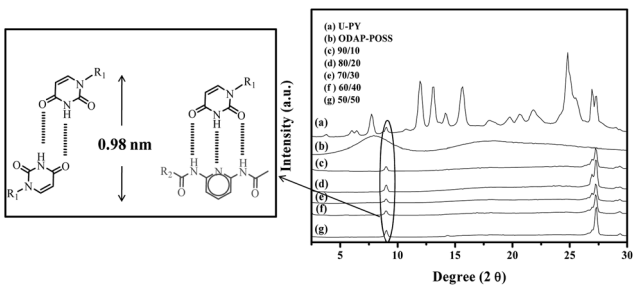

Fig. 3 Wide-angle X-ray diffraction patterns for U-PY/ODAP-POSS complexes in various weight ratios (The distance of U–U and U–DAP interaction is shown in the left part).

spacing of 7.86° (1.12 nm) of all U-PY/ODAP-POSS blends disappears while two reflection peaks with a sequence corresponding to d-spacing of *ca.* 9.0° (d = 0.98 nm) and 27.3° (d = 0.32 nm) appear. This observation indicates that ODAP-POSS associates strongly with its complementary U-PY, and such

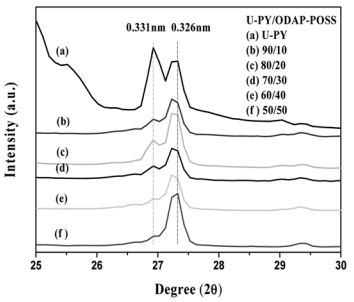

	The relative intensity at 26.9°	The relative intensity at 27.3°
(a)	1.16	1
(b)	0.61	1
(c)	0.59	1
(d)	0.60	1
(e)	0.47	1
(f)	0.27	1

Fig. 4 Wide-angle X-ray diffraction patterns for U-PY/ODAP-POSS composites in various weight ratios at the 2θ range of 25–30° (the relative intensities at 26.9° and 27.3° are shown on the right).

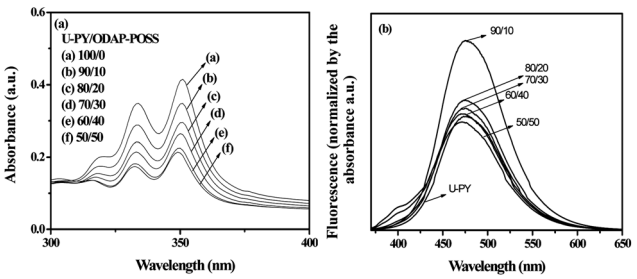

Fig. 5 UV-Vis (a) and photoluminescence spectra (b) of U-PY/ODAP-POSS composites in films.

U–DAP interaction is more favorable than either DAP–DAP or U–U interaction (Scheme 2). In addition, the intensity of π–π stacking aggregation in the pyrene–pyrene layer gradually decreases (26.9°, d = 0.33 nm) with increasing content of ODAP-POSS (Fig. 4), reflecting the high complementary of this system. Thus, the incorporation of ODAP-POSS acts as an effective retarder of pyrene–pyrene aggregation formation in U–DAP

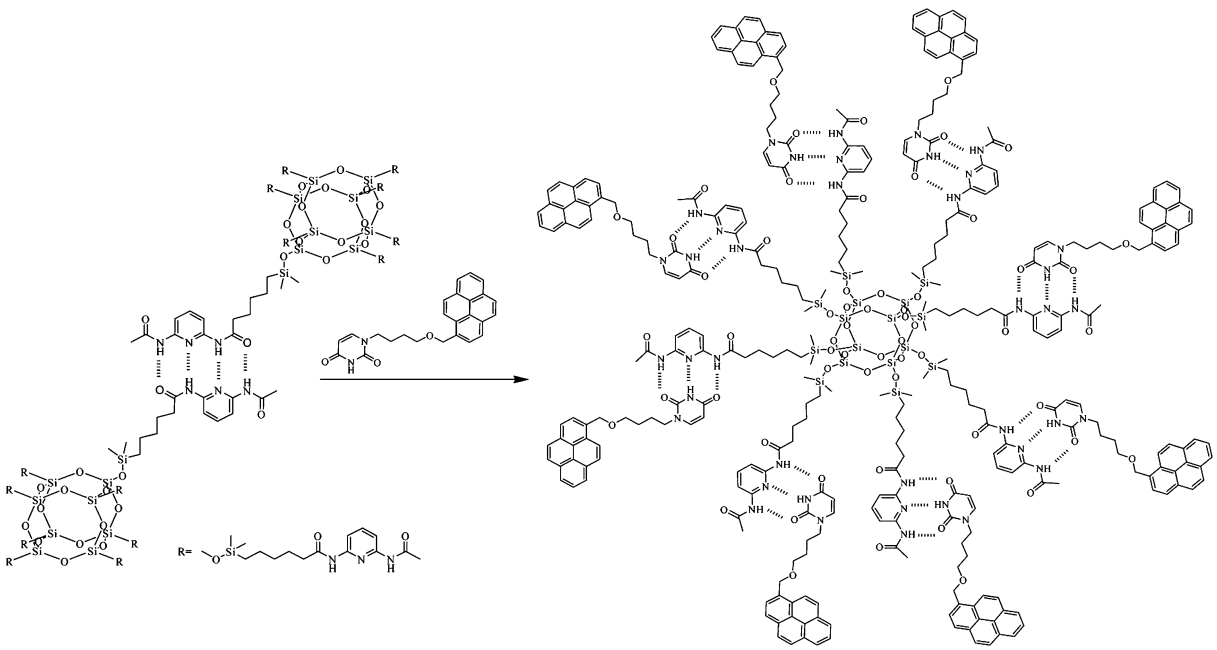

Scheme 2 Self-assembled formed from U-PY/ODAP-POSS complexes.

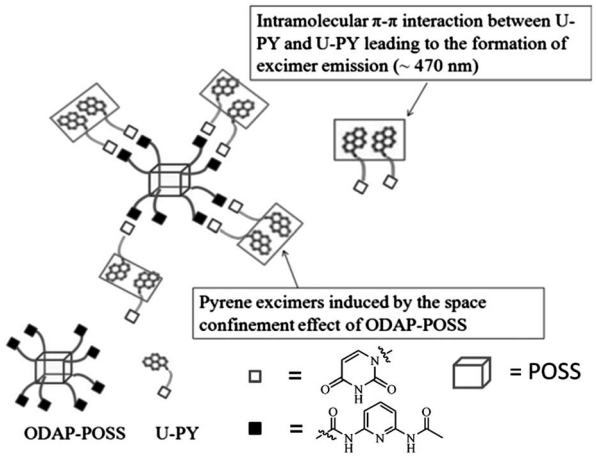

Scheme 3 The emission formation in U-PY and U-PY/ODAP-POSS.

interaction. Therefore, ODAP-POSS appears to have potential applications in improving the quantum efficiency (QE) of U-PY through blending.

Optical and electroluminescence properties of U-PY/ODAP-POSS

Fig. 5 presents the UV-Vis and PL spectra of U-PY/ODAP-POSS in solid films, where the thin films were fabricated on glass slides through the spin-coating method using tetrachloroethane as solvent. The maximum absorptions of U-PY are 319, 333 and 351 nm in the UV-Vis spectra and 477 nm in the PL spectra. The shape of the PL emission spectrum of U-PY/ODAP-POSS blend is slightly different to that of U-PY, the emission wavelength is slightly blue-shifted (from 477 nm to 472 nm) due to the presence of POSS cage interrupting the aggregation of the pyrene groups. Surprisingly, the intensities of pyrene excimer are significantly increased by introducing ODAP-POSS, probably due to the formation of intramolecular π–π interaction (pyrene–pyrene) and the space confinement effect of ODAP-POSS (Scheme 3). The PLQE of U-PY is 0.68, which is substantially higher than that of pyrene (Q = 0.44)[52] (Table 1). The PLQE of U-PY/ODAP-POSS (90/10) is further raised to 0.97. Increasing the ODAP-POSS content from 10 wt% to 20 wt%, the PLQE of U-PY/ODAP-POSS began to decrease. It is probably because ODAP-POSS will aggregate by itself and quench the PLQE of U-PY/ODAP-POSS. The PLQE of U-PY/ODAP-POSS is

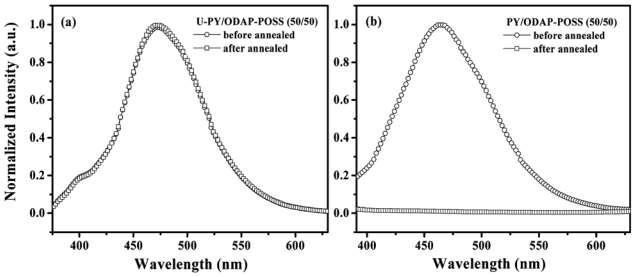

Fig. 6 Thermal quenching of U-PY and PY/ODAP-POSS in films after annealing at 150 °C.

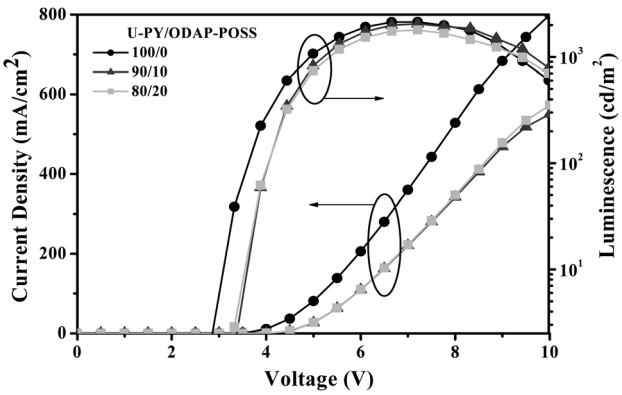

Fig. 7 *I–V–L* characteristics of ITO/PEDOT:PSS/LEM/TPBI/LiF/Al devices.

measured by an integrating sphere in solid state, and the PLQE measured by relative method also agreed well with the integrating sphere results. Most importantly, these U-PY groups "bound" to ODAP-POSS are well separated by the POSS cage and thus the quantum yield of U-PY can be significantly improved. In previous reports,[53,54] pyrene in pyrene-based films tends to degrade at temperatures well below its boiling point (393 °C), therefore, its applications in OLEDs are limited. Surprisingly, the incorporation of ODAP-POSS into U-PY results in improved thermal and color stabilities. Fig. S4† displays thermal quenching of U-PY/ODAP-POSS composites in films after annealing at 150 °C. For direct comparison, thermal annealing of films of U-PY/ODAP-POSS and PY/ODAP-POSS were carried out. The PL spectra (Fig. 6a) reveal that the emission peak at 472 nm of the 50/50 U-PY/ODAP-POSS blend

Table 1 The compositions and optical properties of U-PY/ODAP-POSS[c]

Blend U-PY/ODAP-POSS	Solution		Thin film		Thin film	
	A_{max} (nm)	PL_{max} (nm)	A_{max} (nm)	PL_{max} (nm)	Φ_{PL}(%)[a]	Φ_{PL}(%)[b]
100/0	329,346	382,397	333,351	477	68	1
90/10	329,346	382,397	333,350	476	97	1.6
80/20	329,346	382,397	333,350	474	73.6	1.14
70/30	329,346	382,397	332,349	474	70.6	1.07
60/40	329,346	382,397	332,349	474,400	70	1.03
50/50	329,346	382,397	332,349	472,400	48	0.92

[a] Absolute quantum yield of the thin film measured by an integrating sphere. [b] Relative quantum yields were measured by taking U-PY to be 1.0 for comparison. [c] The fluorescence quantum efficiency Φ_{PL} (%) of pyrene in thin film is 44%.

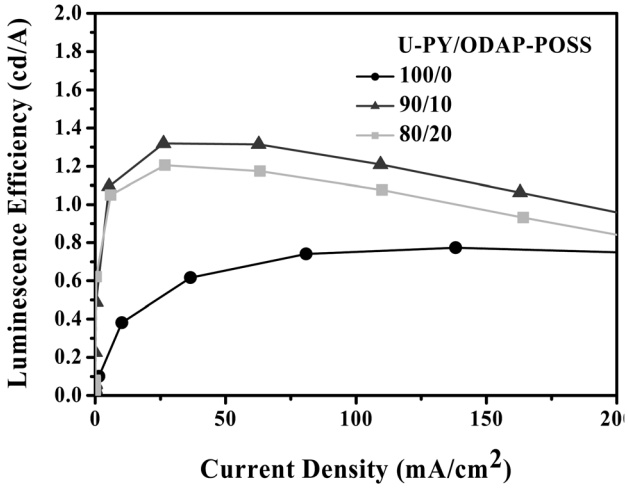

Fig. 8 Plot of LE with respect to current density for the ITO/PEDOT:PSS/LEM/TPBI/LiF/Al devices.

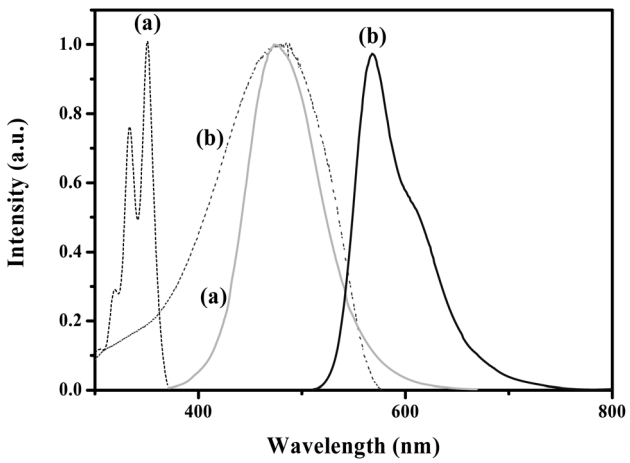

Fig. 9 Absorption (dotted lines) and PL (solid lines) spectra of (a) U-PY/ODAP-POSS (90/10) and (b) MEH-PPV in solid films.

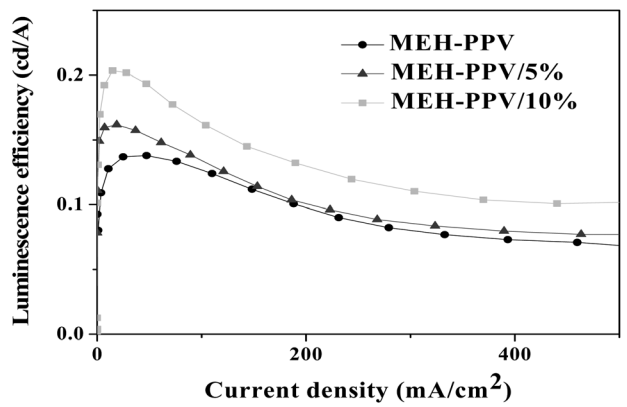

Fig. 10 Current density–luminescence efficiency characteristics of MEH-PPV/U-PY/ODAP-POSS (90/10) based device.

remains nearly unchanged after annealing. In contrast, the emission peak of the 50/50 PY/ODAP-POSS blend totally disappears after thermal annealing (Fig. 6b). The intermolecular fixing effect from U–DAP interactions is responsible for the observed color stability improvement during thermal annealing.

The electroluminescence of U-PY/ODAP-POSS in an OLED is blue. An EL device with the configuration ITO/PEDOT:PSS/(U-PY/ODAP-POSS)/TPBI (30 nm)/LiF(15 Å)/Al was fabricated. The PEDOT:PSS was spin-coated on an ITO substrate with a film thickness of 50 nm and then baked at 100 °C for 30 min. The U-PY/ODAP-POSS composite films were coated onto the PEDOT:PSS layer with a film thickness of 50 nm from a tetrachloroethane solution of U-PY/ODAP-POSS. The electroluminescence (EL) spectra of U-PY/ODAP-POSS composite films based OLEDs containing various ODAP-POSS contents are shown in Fig. S5,† respectively. The maximum EL peaks for U-PY/ODAP-POSS (100/0), (90/10) and (80/20) based devices appear at 483, 470 and 468 nm, respectively. The maximum EL emission of U-PY/ODAP-POSS in the solid state coincides with that in PL spectra, whereas the EL emission of U-PY/ODAP-POSS (80/20) is blue shifted as compare to U-PY (from 483 nm to 468 nm), implying that aggregation of both the inter-chain and chromophoric segments was reduced by the presence of the POSS cages. The U-PY/ODAP-POSS based device exhibits significant lower current density than U-PY device at same voltage. The turn-on voltage of the U-PY/ODAP-POSS 90/10 device was 3.7 V with the maximum brightness of 2047 cd m^{-2} at 7.5 V (Fig. 7) and the maximum luminescence efficiency was 1.32 cd A^{-1} at a current density of 26 mA cm^{-2} (Fig. 8). This device exhibited significantly higher luminance efficiency than U-PY because the POSS cages not only suppressed the U-PY aggregation but also reduced current leakage of the device.[55,56] Increasing the ODAP-POSS content from 10 wt% to 20 wt% result in the brightness of the U-PY/ODAP-POSS-based device decreased slightly because of an increase in the resistivity of the light emitting layer. However, these results indicate that the U-PY/ODAP-POSS appears to have potential to be used in improving device efficiency through simple blending because the high quantum efficiency of U-PY/ODAP-POSS. In addition, the U-PY/ODAP-POSS has good solution processing properties. The effect of the incorporation of U-PY/ODAP-POSS on the photoluminescence properties of the MEH-PPV was measured. The emission peaks of the U-PY/ODAP-POSS (90/10) at 476 nm and the MEH-PPV at 568 nm correspond to the wavelengths of the blue and orange emitters present in this system (Fig. 9), the maximum absorption of wavelength of MEH-PPV in solid film coincides with the maximum emission wavelength of U-PY/ODAP-POSS (90/10) in solid film, indicating a significant potential for Förster energy transfer. The characteristic curve and EL spectra of the U-PY/ODAP-POSS 90/10-doped MEH-PPV devices are shown in Fig. S6 and S7,† respectively. The luminance efficiencies of the U-PY/ODAP-POSS 90/10-doped MEH-PPV devices are in the range of 0.16–0.20 cd A^{-1} (Fig. 10), 1.16–1.45 times higher than that of MEH-PPV (0.138 cd A^{-1}), implying that energy transfer efficiency from the pyrene groups on U-PY/ODAP-POSS to MEH-PPV is significantly enhanced.

Conclusions

A new supramolecular light-emitting material has been developed through incorporation of a triple hydrogen bonding array between U-PY and ODAP-POSS as an electroluminescent

material. This novel POSS derivative has good thermal stability, fluorescence efficiency and good solution processing properties. The U-PY/ODAP-POSS also behaves as an effective dopant to enhance energy transfer from itself to MEH-PPV. In addition, U-PY(90 wt%)/ODAP-POSS (10 wt%)-doped MEH-PPV devices exhibited high luminance efficiency, 1.45 times greater than that of MEH-PPV. As noted above, all these results confirm that the incorporation of U-PY/ODAP-POSS into the MEH-PPV is an effective and potential route towards next-generation, high-efficiency LED devices.

Experimental section

Characterization

FTIR spectroscopy. Recorded using a Nicolet Avatar 320 FTIR spectrometer; 32 scans were collected at a spectral resolution of 1 cm^{-1}. The conventional KBr disk method was employed: the sample was dissolved in tetrachloroethane, then cast onto a KBr disk, and dried under vacuum at 70 °C.

Nuclear magnetic resonance spectroscopy. ^{1}H and ^{13}C NMR spectra were recorded at 300 and 75 MHz, respectively, using a Varian Inova 300 MHz spectrometer equipped with a 9.395-T Bruker magnet. The samples (*ca.* 5 mg for ^{1}H NMR; *ca.* 20 mg for ^{13}C NMR) were dissolved in deuterated solvent and analyzed at room temperature.

Matrix-assisted laser desorption/ionization time-of-flight mass spectrometry. MALDI-TOF mass spectra were recorded using a Bruker AutoFlex spectrometer equipped with a 337 nm N_2 laser (over 20 Hz).

Thermogravimetric analysis. TGA was performed using a TA Instruments TGA 2050 thermogravimetric analyzer operated at a heating rate of 20 °C min^{-1} from room temperature to 800 °C under a continuous flow of nitrogen.

Differential scanning calorimetry. DSC was performed using a DuPont 910 DSC-9000 controller operated under an atmosphere of dry N_2. The samples were weighed (*ca.* 5–10 mg) and sealed in an aluminum pan, and then heated from 0 to 100 °C at a rate of 20 °C min^{-1}. The glass transition temperature was taken as the midpoint of the heat capacity transition between the upper and lower points of the deviation from the extrapolated glass and liquid lines.

Wide-angle X-ray diffraction. WAXD spectra of powders were obtained using a Rigaku D/max-2500 X-ray diffractometer. The radiation source was Ni-filtered Cu-Kα radiation at a wavelength of 0.154 nm. The voltage and current were set at 30 kV and 20 Ma, respectively. The sample was mounted on a circular sample holder; the data were collected using a proportional counter detector over the range from 2 to 40° at a rate of 5° min^{-1}. Bragg's law ($\lambda = 2d \sin\theta$) was used to compute the d-spacing corresponding to the complementary behavior.

UV-Vis and photoluminescence (PL) spectra. UV-Vis and photoluminescence (PL) spectra were measured using an HP 8453 diode-array spectrophotometer and a Hitachi F-4500 luminescence spectrometer, respectively. Absolute quantum yield was measured by an integrating sphere of HORIBA JOBIN YVON Fluorolog-3 PL spectrometer.

Light-emitting devices. The EL devices were fabricated through vacuum deposition of the materials at 10^{-6} torr onto ITO glass with a sheet resistance of 25 Ω $square^{-1}$. All of the organic layers were deposited at a rate of 1.0 Å s^{-1}. The cathode was completed through thermal deposition of LiF at a deposition rate of 0.1 Å s^{-1}, then capped with Al metal through thermal evaporation at a rate of 4.0 Å s^{-1}. The relationships of the current density and brightness of the devices with respect to voltage were measured using a Keithley 2400 source meter and a Newport 1835C optical meter equipped with an 818ST silicon photodiode. The EL spectrum was obtained using a Hitachi F4500 luminescence spectrometer. PLED Devices were fabricated in the configuration ITO/poly(3,4-ethylene dioxythiophene) (PEDOT, 35 nm)/polymer (*ca.* 30 nm)/Ca (50 nm)/Al (100 nm). The PEDOT layer was used as a hole injection layer to facilitate hole conduction, and also to smoothen the relatively rough ITO layer. The TPBI layer deposited through thermal evaporation was employed as an electron-transporting and hole-blocking layer.

Preparation of compounds

Platinum-divinyltetramethyldisiloxane complex (Pt-dvs, the hydrosilylation catalyst) were obtained from Aldrich (USA). Octakis(dimethylsilyloxy)-POSS (Ot-POSS) was purchased from Hybrid Plastics (USA). Poly(2-methoxy,5-(2′-ethyl-hexyloxy)-*i*-phenylene-vinylene) (MEH-PPV) was synthesized through Gilch polymerizations with potassium tertbutoxide in THF solution. All solvents were purchased from TEDIA (USA) and distilled over CaH_2 prior to use. All other chemicals were used as received without purification.

Synthesis of 1-((4-bromobutoxy)methyl)pyrene (1). NaH (2.08 g, 86 mmol) was added to a solution of 1-pyrenemethanol (1.0 g, 4.3 mmol) in dry THF under N_2 atmosphere at room temperature. The mixture was stirred for 0.5 h. Then 1,4-dibromobutane (5.14 ml, 43 mmol) was added and stirred for 48 h. The solvent was removed by vacuum evaporation, and water was carefully added to the reaction mixture to quench the unreacted NaH. The solution was extracted with CH_2Cl_2 (3 × 50 mL), and the combined organic layer was washed with 5% aqueous HCl (50 mL), 10% aqueous Na_2CO_3 (50 mL) and finally with water, and then was dried over by anhydrous $MgSO_4$. The residue after removal of the solvents was chromatographed on silica gel with ethyl acetate/hexane (1 : 10, v/v) as eluent to give white solid (1.185 g, 75%). ^{1}H NMR (300 MHz, $CDCl_3$, ppm):1.765–1.833 (m, 2H), 1.917–1.989 (m, 2H), 3.389 (t, 2H), 3.619 (t, 2H), 5.197 (s, 2H), 7.986–8.044 (m, 4H), 8.121–8.203 (m, 4H), 8.325–8.356 (m, 1H);^{13}C NMR (75 MHz, $CDCl_3$, ppm):28.394, 29.686, 33.803, 69.295, 71.570, 123.377, 124.466, 125.213, 125.931, 126.897, 127.395, 127.690, 131.223, 131.266.

Synthesis of 4-uracilbutyl-1-methylpyrene ether (U-PY) (2). Uracil (0.54 g, 4.8 mmol) was added to a solution of anhydrous K_2CO_3 (0.64 g, 4.8 mmol) in dry DMF. The mixture was stirred

for 0.5 h. Then compound 1 (1.18 g, 3.2 mmol) was added to the solution and stirred at 70 °C for 48 h. Finally, the reaction mixture was filtered, the solvent evaporated, and the solid washed several time with water. The residue after removal of the solvents was chromatographed on silica gel with ethyl acetate/hexane (1: 3, v/v) as eluent to give white solid (0.48g, 37%). m.p. 86 °C; ^{1}H NMR (300 MHz, $CDCl_3$, ppm):1.599–1.723 (m, 4H), 3.515–3.627 (m, 4H), 5.176 (s, 2H), 5.300–5.333 (d, 1H), 6.675–6.701 (d, 1H), 7.953–8.039 (m, 4H), 8.111–8.201 (m, 4H), 8.329–8.360 (m, 1H), 8.791 (br, 1H);^{13}C NMR (75 MHz, $CDCl_3$, ppm):25.952, 26.356, 48.338, 69.416, 71.669, 101.647, 123.383, 124.409, 124.571, 124.857, 125.249, 125.310, 126.031, 127.129, 127.319, 127.463, 127.693, 129.289, 130.638, 131.130, 144.354, 150.757, 163.808;IR (KBr): 3175, 3049, 2938, 2863, 1676, 1456, 1090, 845 cm^{-1}; UV-Vis (tetrachloroethane):λ_{max} = 329,346 nm; MS (EI), *m/z* [M^+]: 398, calcd: 398.16; Elem. Anal: calcd (%) for $C_{25}H_{22}N_2O_3$: C, 75.36; H, 5.57; N,7.03. Found: C, 74.99; H, 5.09; N, 7.06.

Synthesis of *N*-(6-aminopyridin-2-yl)hex-5-enamide (3). A solution of 5-hexenoic acid (1.00 g, 8.67 mmol) in dry CH_2Cl_2 (10 mL) was treated with $SOCl_2$ (3 mL) and heated at reflux for 1 h under argon. After cooling to room temperature, the reaction mixture was concentrated under reduced pressure and the residue was dried under vacuum for 5 h to remove traces of $SOCl_2$. The resulting residue was dissolved in dry THF (4 mL) and treated dropwise with a solution of 2,6-diaminopyridine (4.78 g, 43.8 mmol) and triethylamine (3.6 ml, 26.3 mmol) in THF (10 mL). The mixture was stirred overnight at 0 °C under argon. The solvent was removed under reduced pressure, the residue was treated with water (10 mL), washed with CH_2Cl_2 (30 mL). The mixture was extracted with CH_2Cl_2 (30 mL) and the combined organic layers were dried with $MgSO_4$. The residue after removal of the solvents was chromatographed on silica gel with ethyl acetate/hexane (2 : 3, v/v) as eluent to give compound **3** (1.2 g, 68%). ^{1}H NMR(300 MHz, $CDCl_3$, ppm):1.742–1.816 (m, 2H), 2.014–2.118 (m, 2H), 2.276–2.326 (t, 2H), 4.322 (br, 2H), 4.938–5.030 (m, 2H), 5.676–5.810 (m, 1H), 6.197–6.223 (m, 1H), 7.384–7.436 (m, 1H), 7.495–7.521 (m, 1H), 7.831 (br, 1H);^{13}C NMR(75 MHz, $CDCl_3$, ppm):24.321, 32.962, 36.790, 103.234, 104.145, 115.442, 137.627, 140.116, 149.774, 157.004, 171.280.

Synthesis of octakis[dimethyl(*N*-(6-aminopyridin-2-yl))siloxy] silsesquioxane (4). A solution of Pt–dvs (0.1 mL, 200 ppm) was injected *via* syringe into a solution of Ot-POSS (0.5 g, 0.49 mmol) and compound **3** (1.2 g, 5.85 mmol) in dry toluene (14 mL). The mixture was stirred at 80 °C under an argon atmosphere until the Si–H peak (2140 cm-1) disappeared completely (4 h). After cooling to room temperature, the mixture was filtered, the solvent evaporated, and the residue purified through chromatography (SiO_2; MeOH) to give compound **4** (0.73g, 56%). ^{1}H NMR (300 MHz, $CDCl_3$, ppm):0.057–0.099 (m, 48H), 0.491–0.545 (m, 16H), 1.298–1.391 (m, 32H), 1.615–1.639 (m, 16H), 2.272–2.325 (m, 16H), 4.408–4.468 (m, 16H), 6.185–6.209 (m, 8H), 7.378–7.524 (m, 8H), 7.6 (m, 8H), 8.4 (m, 8H);^{13}C NMR(75 MHz, $CDCl_3$, ppm:−0.357, 0.998, 17.472, 22.685, 25.162, 32.882, 37.578, 49.172, 104.056, 140.104, 150.129, 157.115, 172.015.

Synthesis of octakis[dimethyl(*N*-(6-acetamidopyridin-2-yl)) siloxy] silsesquioxane (ODAP-POSS) (5). Triethylamine (0.343 ml, 2.46 mmol) was added to a solution of compound **4** (654 mg, 0.25 mmol) in dry THF (5.5 ml). The mixture was stirred for 10 min. Then acetyl chloride was added to the solution and stirred at 0 °C for 1.5 h. The solvent was removed under reduced pressure, the residue was treated with water (30 ml). The solution was extracted with ethyl acetate (40 ml) and the organic layers were dried with $MgSO_4$. The residue after remove of the solvents was chromatographed on silica gel with MeOH as eluent to give white solid (0.58g, 79%). ^{1}H NMR (300 MHz, $CDCl_3$, ppm): 0.038–0.062 (m, 6H), 0.518 (m, 2H), 1.296 (m, 4H), 1.623 (m, 2H), 2.094 (s, 3H), 2.285 (m, 2H), 7.572–7.604 (m, 1H), 7.827 (m, 2H), 8.227 (m, 2H);^{13}C NMR (75 MHz, $CDCl_3$, ppm):−0.341, 0.959, 17.318, 22.547, 24.465, 24.865, 32.638, 37.467, 109.528, 140.629, 149.632, 168.921, 172.022;IR (KBr): 3407, 3286, 3211, 3049, 2960, 2924, 2854, 1680, 1580, 1510, 1450, 1100, 845 cm^{-1}; UV-Vis (tetrachloroethane): λ_{max} = 293 nm; MALDI-TOF: *m/z* 2995.166 $[M + Na]^+$.

Acknowledgements

This study was supported financially by the National Science Council, Taiwan (contract no. NSC-99-2120-M-009-008). Our special thanks go to Professor C.-H. Cheng for his support and assistance during the preparation and characterization of the light-emitting devices.

Notes and references

1 W. Saenger, *Principles of Nucleic Acid Structures*, Springer, Berlin, 1984.
2 V. N. Soyfer, V. N. Potaman, *Triple-Helical Nucleic Acids*, Springer, New York, 1995.
3 W. H. Binder and R. Zirbs, *Adv. Polym. Sci.*, 2007, **207**, 1.
4 B. D. Mather, M. B. Baker, F. L. Beyer, M. A. G. Berg, M. D. Green and T. E. Long, *Macromolecules*, 2007, **40**, 6834.
5 R. Shenhar, H. Xu, B. L. Frankamp, T. E. Mates, A. Sanyal, O. Uzun and V. M. Rotello, *J. Am. Chem. Soc.*, 2005, **127**, 16318.
6 W. H. Binder, C. Kluger, C. J. Straif and G. Friedbacher, *Macromolecules*, 2005, **38**, 9405.
7 T. Kato, H. Kihara, S. Ujiie, T. Uryu and J. M. J. Fréchet, *Macromolecules*, 1996, **29**, 8734.
8 S. Rieth, C. Baddeley and J. D. Badjic, *Soft Matter*, 2007, **3**, 137.
9 S. Sivakova and S. J. Rowan, *Chem. Soc. Rev.*, 2005, **34**, 9.
10 K. Yamauchi, J. R. Lizotte and T. E. Long, *Macromolecules*, 2002, **35**, 8745.
11 E. Snip, S. Shinkai and D. N. Reinhoudt, *Tetrahedron Lett.*, 2001, **42**, 2153.
12 I.-H. Lin, C.-C. Cheng, Y.-C. Yen and F.-C. Chang, *Macromolecules*, 2010, **43**, 1245.
13 T. Kato, *Supramol. Sci.*, 1996, **3**, 53.
14 A. K. Boal, T. H. Galow, F. Ilhan and V. M. Rotello, *Adv. Funct. Mater.*, 2001, **11**, 461.
15 T. H. Galow, F. Ilhan, G. Cooke and V. M. Rotello, *J. Am. Chem. Soc.*, 2000, **122**, 3595.
16 R. J. Thibault, T. H. Galow, E. J. Turnberg, M. Gray, P. J. Hotchkiss and V. M. Rotello, *J. Am. Chem. Soc.*, 2002, **124**, 15249.
17 K. Das, H. Nakade, J. Penelle and V. M. Rotello, *Macromolecules*, 2004, **37**, 310.
18 R. Shenhar, A. Sanyal, O. Uzun, H. Nakade and V. M. Rotello, *Macromolecules*, 2004, **37**, 4931.
19 R. P. Sijbesma, F. H. Beijer, L. Brunsveld, B. J. B. Folmer, J. H. K. K. Hirschberg, R. F. M. Lange, J. K. L. Lowe and E. W. Meijer, *Science*, 1997, **278**, 1601.
20 F. H. Beijer, R. P. Sijbesma, H. Kooijman, A. L. Spek and E. W. Meijer, *J. Am. Chem. Soc.*, 1998, **120**, 6761.
21 B. J. B. Folmer, R. P. Sijbesma, H. Kooijman, A. L. Spek and E. W. Meijer, *J. Am. Chem. Soc.*, 1999, **121**, 9001.

22 J. H. K. K. Hirschberg, F. H. Beijer, H. A. van Aert, P. C. M. M. Magusin, R. P. Sijbesma and E. W. Meijer, *Macromolecules*, 1999, **32**, 2696.
23 R. F. M. Lange, M. van Gurp and E. W. Meijer, *J. Polym. Sci., Part A: Polym. Chem.*, 1999, **37**, 3657.
24 L. Zhang, H. C. L. Abbenhuis, Q. Yang, Y. M. Wang, P. C. M. M. Magusin, B. Mezari, R. A. van Santen and C. Li, *Angew. Chem., Int. Ed.*, 2007, **46**, 5003.
25 S. H. Phillips, T. S. Haddad and S. J. Tomczak, *Curr. Opin. Solid State Mater. Sci.*, 2004, **8**, 21.
26 E. Jeoung, J. B. Carroll and V. M. Rotello, *Chem. Commun.*, 2002, 1510.
27 D. Neumann, M. Fisher, L. Tran and J. G. Matisons, *J. Am. Chem. Soc.*, 2002, **124**, 13998.
28 J. Choi, R. Tamaki, S. G. Kim and R. M. Laine, *Chem. Mater.*, 2003, **15**, 3365.
29 J. Livage, *Bull. Mater. Sci.*, 1999, **22**, 201.
30 C. Sanchez, G. J. de A. A. Soler-Illia, F. Ribot, T. Lalot, C. R. Mayer and V. Cabuil, *Chem. Mater.*, 2001, **13**, 3061.
31 J. Pyun and K. Matyjaszewki, *Chem. Mater.*, 2001, **13**, 3436.
32 U. Schubert, *Chem. Mater.*, 2001, **13**, 3487.
33 G. Wu and Z. Su, *Chem. Mater.*, 2006, **18**, 3726.
34 S. Y. Lu and I. Hamerton, *Prog. Polym. Sci.*, 2002, **27**, 1661.
35 R. O. R. Costa, W. L. Vasconcelos, R. Tamaki and R. M. Laine, *Macromolecules*, 2001, **34**, 5398.
36 C. M. Brick, R. Tamaki, S. G. Kim, M. Z. Asuncion, M. Roll, T. Nemoto, Y. Ouchi, Y. Chujo and R. M. Laine, *Macromolecules*, 2005, **38**, 4655.
37 C. M. Brick, Y. Ouchi, Y. Chujo and R. M. Laine, *Macromolecules*, 2005, **38**, 4661.
38 S. Xiao, M. Nguyen, X. Gong, Y. Cao, H. Wu, D. Moses and A. J. Heeger, *Adv. Funct. Mater.*, 2003, **13**, 25.
39 W. J. Lin, W. C. Chen, W. C. Wu, Y. H. Niu and A. K. Y. Jen, *Macromolecules*, 2004, **37**, 2335.
40 A. Sellinger, R. Tamaki, R. M. Laine, K. Ueno, H. Tanabe, E. Williams and G. E. Jabbour, *Chem. Commun.*, 2005, 3700.
41 H. J. Cho, D. H. Hwang, J. I. Lee, Y. K. Jung, J. H. Park, J. Lee, S. K. Lee and H. K. Shim, *Chem. Mater.*, 2006, **18**, 3780.
42 J. D. Froehlich, R. Young, T. Nakamura, Y. Ohmori, S. Li, A. Mochizuki, M. Lauters and G. E. Jabbour, *Chem. Mater.*, 2007, **19**, 4991.
43 Y. Xiao, L. Liu, C. He, W. S. Chin, T. Lin, K. Y. Mya, J. Huang and X. Lu, *J. Mater. Chem.*, 2006, **16**, 829.
44 X. Yang, J. D. Froehlich, H. S. Chae, S. Li, A. Mochizuki and G. E. Jabbour, *Adv. Funct. Mater.*, 2009, **19**, 2623.
45 M. Y. Lo, C. Zhen, M. Lauters, G. E. Jabbour and A. Sellinger, *J. Am. Chem. Soc.*, 2007, **129**, 5808.
46 C.-C. Cheng, Y.-C. Yen and F.-C. Chang, *Macromol. Rapid Commun.*, 2011, **32**, 927.
47 C.-C. Cheng, C.-F. Huang, Y.-C. Yen and F.-C. Chang, *J. Polym. Sci., Part A: Polym. Chem.*, 2008, **46**, 6416.
48 J. Gu, J. Wang, J. Leszczynski, Y. Xie and H. F. Schaefer III, *Chem. Phys. Lett.*, 2008, **459**, 164.
49 F. M. Winnik, *Chem. Rev.*, 1993, **93**, 587.
50 M. Kimura, N. Miki, D. Suzuki, N. Adachi, Y. Tatewaki and H. Shirai, *Langmuir*, 2009, **25**, 776.
51 J. Miao and L. Zhu, *Chem. Mater.*, 2010, **22**, 197.
52 Z. Zhao, S. Chen, J. W. Y. Lam, Z. Wang, P. Lu, F. Mahtab, H. H. Y. Sung, I. D. Williams, Y. Ma, H. S. Kwok and B. Z. Tang, *J. Mater. Chem.*, 2011, **21**, 7210.
53 B. J. Basu, C. Anandan and K. S. Rajam, *Sens. Actuators, B*, 2003, **94**, 257.
54 W. Xu, R. Schmidt, M. Whaley, J. N. Demas, B. A. DeGraff, E. K. Karikari and B. A. Famer, *Anal. Chem.*, 1995, **67**, 3172.
55 R. H. Lee and H. H. Lai, *Eur. Polym. J.*, 2007, **43**, 715.
56 J. M. Kang, H. J. Cho, J. Lee, J. I. Lee, S. K. Lee, N. S. Cho, D. H. Hwang and H. K. Shim, *Macromolecules*, 2006, **39**, 4999.

